



CHEMISTRY

A European Journal



Accepted Article

Title: Triangular-shaped $\text{La}_2\text{O}_2\text{CO}_3$ Nanosheets Supported Pd Nanoparticles: A New Highly Efficient and Durable Catalyst for Selective Hydrogenation of Cinnamaldehyde to Hydrocinnamaldehyde

Authors: Fei Wang, Yanshuai Bi, Kai Hu, and Xuejiao Wei

This manuscript has been accepted after peer review and appears as an Accepted Article online prior to editing, proofing, and formal publication of the final Version of Record (VoR). This work is currently citable by using the Digital Object Identifier (DOI) given below. The VoR will be published online in Early View as soon as possible and may be different to this Accepted Article as a result of editing. Readers should obtain the VoR from the journal website shown below when it is published to ensure accuracy of information. The authors are responsible for the content of this Accepted Article.

To be cited as: *Chem. Eur. J.* 10.1002/chem.202000741

Link to VoR: <http://dx.doi.org/10.1002/chem.202000741>

Supported by
ACES

WILEY-VCH

Triangular-shaped $\text{La}_2\text{O}_2\text{CO}_3$ Nanosheets Supported Pd Nanoparticles: A New Highly Efficient and Durable Catalyst for Selective Hydrogenation of Cinnamaldehyde to Hydrocinnamaldehyde

Fei Wang,^{*[a]} Yanshuai Bi,^[a] Kai Hu,^[a] and Xuejiao Wei^{*[b]}

Dedication ((optional))

[a] Dr. Fei Wang, Yanshuai Bi, Kai Hu
Advanced Catalysis and Green Manufacturing Collaborative Innovation Center
Changzhou University
21 Gehu Road, Changzhou 213164 (China)
E-mail: wangfei@cczu.edu.cn

[b] Dr. Xuejiao Wei
School of Chemical Engineering and Materials
Changzhou Institute of Technology
666 Liaohe Road, Changzhou 213022 (China)

E-mail: weixj@czu.cn

Supporting information for this article is given via a link at the end of the document. ((Please delete this text if not appropriate))

Abstract: A triangular-shaped $\text{La}_2\text{O}_2\text{CO}_3$ nanosheets exposed the predominant (001) planes supported Pd catalyst ($\text{Pd}/\text{La}_2\text{O}_2\text{CO}_3\text{-TNS}$) was successfully prepared using a facile solvothermal method. $\text{Pd}/\text{La}_2\text{O}_2\text{CO}_3\text{-TNS}$ catalysts not only exhibited excellent catalytic activity and recycling stability for hydrogenation of cinnamaldehyde (CAL) to hydrocinnamaldehyde (HCAL) with TOF of up to 41238 h^{-1} . This enhanced activity of $\text{Pd}/\text{La}_2\text{O}_2\text{CO}_3\text{-TNS}$ resulted from strong metal-support interactions (SMSI). Structure analysis and characterization demonstrated that surface oxygen-enriched $\text{La}_2\text{O}_2\text{CO}_3\text{-TNS}$ supports exposed (001) planes was beneficial to charge transfer between the Pd nanoparticles and triangle-shaped $\text{La}_2\text{O}_2\text{CO}_3$ nanosheets and increases the electron density of Pd. Moreover, the modulated electron states of the $\text{Pd}/\text{La}_2\text{O}_2\text{CO}_3\text{-TNS}$ catalysts can enhance the adsorption and activation of hydrogen, leading to the enhanced hydrogenation activity.

Introduction

Supported metal catalysts are the most widely used catalysts in several important chemical processes and chemical industries because of high thermal stability, high dispersion of active centers and excellent cyclic stability.^[1] Most of the supported metal catalysts^[2] use reducible metal oxides (such as CeO_2 ^[3], Co_3O_4 ^[4], Fe_2O_3 ^[5], MnO_2 ^[6], etc.) and acid-base metal oxides (Al_2O_3 ^[7], MgO ^[8], La_2O_3 ^[9], CaO ^[10], etc.) as supports. The role of oxide supports is mainly embodied in immobilization of the active component and improvement of the metal dispersion and surface area.^[11-13] In recent years, many reports have shown that the catalytic activity of supported metal catalysts can be adjusted by the particle size, shape and composition of the material concerned.^[14-16] Zhang et al.^[17] reported Pd clusters

with a high dispersion of 73.6 % dispersed on porous nanorods of CeO_2 catalyst exhibit the highest catalytic activity and best chemoselectivity for hydrogenation of nitroarenes. Tan et al.^[18] presented the {100}-faceted CeO_2 nanocubes supported Pd nanoparticles catalysts exhibited much higher activity than those {111}-faceted ceria nanooctahedrons and nanorods (enclosed by {100} and {111} facets) supported Pd nanoparticles for formaldehyde Oxidation. The same example can be also found for acid-base oxides supports. Huang et al.^[19] reported the shape effect significantly modified basicity of $\text{La}_2\text{O}_2\text{CO}_3$ and improves the performance of $\text{Ir}/\text{La}_2\text{O}_2\text{CO}_3$ catalyst in the steam reforming of glycerol at high temperatures up to $650 \text{ }^\circ\text{C}$ toward a sustainable hydrogen production.

Previous reports found that physicochemical interactions generated by these associations between the metal and the support can also influence catalytic properties, which have been linked to the strong metal-support interaction (SMSI).^[20-23] Guo et al.^[24] altered the size regimes of the Ru deposits in Ru/CeO_2 assemblies and uncovered the competitive relationship between SMSI. And Shen et al.^[25] reported that Cu/CeO_2 catalysts are highly active for the low-temperature water-gas shift and revealed that the reaction occurs at the copper-ceria interfacial perimeter due to SMSI. However, from the recent literatures we found that most of these SMSI phenomena mainly occur on reducible oxides, such as CeO_2 ^[26], MnO_2 ^[27], TiO_2 ^[28], et al., which was ascribed to their ability to change oxidation states by exchanging oxygen atoms with the atmosphere and create oxygen vacancies through the surface oxide and oxide crystal.

For acid-base oxide as supports, Shen et al.^[29] prepared Cu nanoparticles dispersed rod-shaped $\text{La}_2\text{O}_2\text{CO}_3$ catalysts. This basic support mainly provided substantial amounts of medium-

strength basic sites for the activation of alcohol and directed the selective dispersion of hemispherical Cu particles. Murata et al.^[30] reported Pd/ θ , α -Al₂O₃ with weak metal-support interaction showed a volcano-shaped dependence of the catalytic activity on the size of Pd particles, and the catalytic activity of the strongly interacted Pd/ γ -Al₂O₃ increased with the particle size. From these results we found that the improvement of catalytic activity is mainly attribute to the acid-base properties of the support and the size of the metal active center. SMSI effect has been rarely reported for basic oxide support.

Herein, a new highly efficient triangular-shaped La₂O₂CO₃ nanosheets (La₂O₂CO₃-TNS) supported Pd catalyst was successfully prepared. The La₂O₂CO₃-TNS mainly exposed (001) planes where oxygen ions terminated (001) surfaces generated a stronger electronic interaction with Pd, which resulted in the highly efficient conversion for cinnamaldehyde (CAL) to hydrocinnamaldehyde (HCAL) with TOF of 41238 h⁻¹. Moreover, after five consecutive cycles Pd/La₂O₂CO₃-TNS still maintain the same activity and selectivity. Structure analysis and characterizations revealed that morphology-induced SMSI between Pd and La₂O₂CO₃-TNS remarkably enhanced the catalytic activity.

Results and Discussion

Figure 1 presented XRD pattern of as-prepared La₂O₂CO₃-TNS support. These peaks at about 26°, 27°, 31°, and 45° for La₂O₂CO₃-TNS can be indexed to (100), (101), (103), and (110) phases, which corresponding to hexagonal phase of La₂O₂CO₃ (JCPDS Card No. 37-0804).^[31] No other peaks were found, indicating that as-prepared sample were pure La₂O₂CO₃ phase. After deposition of Pd, distinguished characteristic peaks due to La₂O₂CO₃ are observed for Pd/La₂O₂CO₃-TNS catalysts. However, no Pd peak was observed, which was probably attributed to the fact that Pd nanoparticles were high-dispersed on surface of La₂O₂CO₃-TNS.

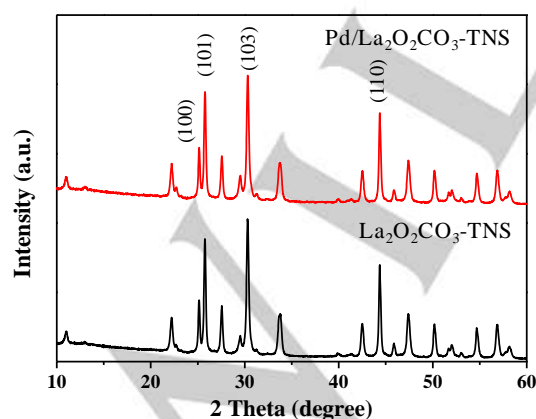


Figure 1. XRD patterns of as-prepared La₂O₂CO₃-TNS and Pd/La₂O₂CO₃-TNS samples.

TEM, SEM and HRTEM images of as-prepared La₂O₂CO₃-TNS were shown in Figure 2. As expected, the La₂O₂CO₃ sheets with triangle shape of regular shape and uniform size were obtained (Figure 2a). Figure 2b showed the typical TEM image of a single triangular-shaped La₂O₂CO₃ nanosheet. Most of the nanosheets were about 300-400 nm in length (the distance from the triangle bottom to the tip). Figure 2c illustrated SEM representative image of as-prepared La₂O₂CO₃-TNS and the thickness of nanosheet is about 22-25 nm. These images confirmed that the La₂O₂CO₃-TNS possess an average bottom width of 22-25 nm and a length up to 300-400 nm. The single nanosheet was therefore explored through HRTEM, as shown in Figure 2d and 2e. Figure 2d showed a highly magnified top-view of La₂O₂CO₃-TNS. The lattice spacings of 0.35 and 0.35 nm with an angle of 60° between the adjacent edges correspond to the (010) plane and (100) plane of hexagonal La₂O₂CO₃, respectively. Fast Fourier transformation (FFT) analysis of them displayed the single-crystalline nature of the nanoplate projected along the [001] direction. From side-view, the distances of 0.80 nm between fringes in Figure 2e are consistent with the (002) planes of La₂O₂CO₃. hence, we propose that La₂O₂CO₃-TNS was composed of two main (001) top and bottom surfaces and three (100), (010) and (110) side faces, while the shape of the La₂O₂CO₃ nanorod was assumed to be a square block that was terminated by two (001) flat planes, two (110) side planes, and two (110) end planes, as illustrated in previous reported.^[29]

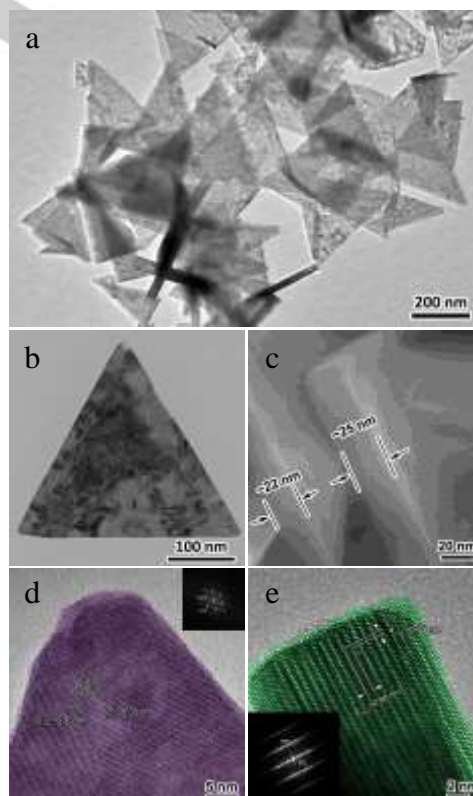


Figure 2. TEM (a, b), SEM (c) and HRTEM (d, e) images of as-prepared La₂O₂CO₃ triangular nanosheets.

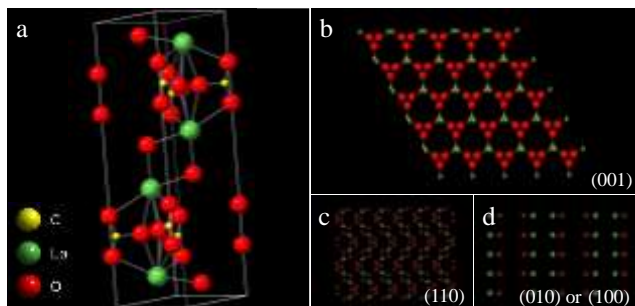


Figure 3. (a) Hexagonal unit of $\text{La}_2\text{O}_2\text{CO}_3$ crystal. Perspective views from (b) (001), (c) (110), (d) (010) or (100) planes of the crystal structure of $\text{La}_2\text{O}_2\text{CO}_3$.

Previous reported presented that $\text{La}_2\text{O}_2\text{CO}_3$ has a hexagonal structure where each La^{3+} cation is surrounded by seven oxygen anions: four in tetrahedral and three in octahedral coordinations (Figure 3a).^[29] As mentioned above, $\text{La}_2\text{O}_2\text{CO}_3$ -TNS was constructed by in-plane (001) surfaces and side (100), (010) and (110) planes. Density-functional theory calculations identified that the {110}, {010} and {100} planes were made up of O and La atoms whereas the {001} plane contained O and C atoms only (Figure 3b-d). The surface area of the {001} planes was about 70 % of the total surface area, so $\text{La}_2\text{O}_2\text{CO}_3$ -TNS mainly exposed (001) plane, made up of O and C atoms, while for the (110) plane of $\text{La}_2\text{O}_2\text{CO}_3$ -NR takes up 40 percent of the total surface.^[29]

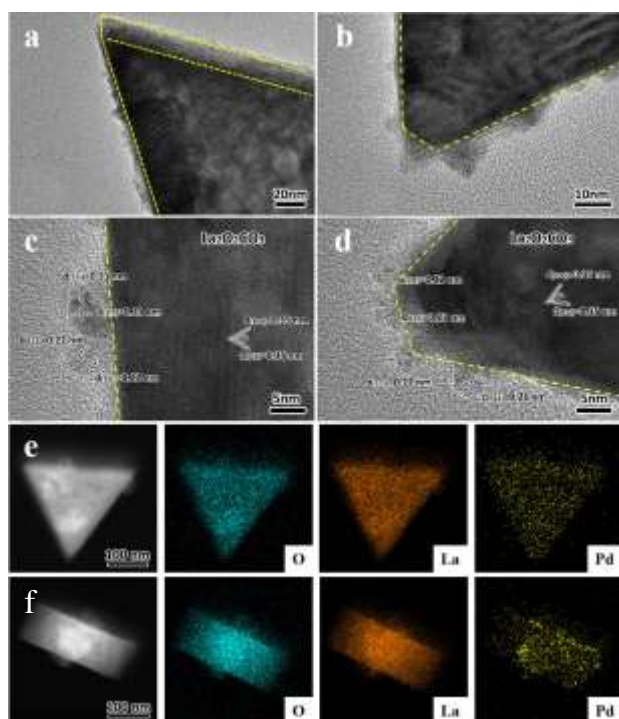


Figure 4. (a, b, c, d) HRTEM images of as-prepared $\text{Pd}/\text{La}_2\text{O}_2\text{CO}_3$ -TNS. HAADF-STEM images and corresponding EDX-elemental mapping images (e) top-view and (f) side-view of $\text{Pd}/\text{La}_2\text{O}_2\text{CO}_3$ -TNS on edge of carbon lattice.

A closer examination of the as-obtained $\text{Pd}/\text{La}_2\text{O}_2\text{CO}_3$ -TNS catalyst by high-resolution TEM (HRTEM) images showed that Pd nanoparticles are uniformly dispersed on $\text{La}_2\text{O}_2\text{CO}_3$ -TNS with regular shape and no significant formation of aggregates was found (Figure 4a-d). These images reveal that size of Pd nanoparticles was about 4-5 nm. The lattice distance with a spacing of 0.22 nm and 0.35 nm correspond to the (111) plane of metallic Pd and the (010) and (100) planes of $\text{La}_2\text{O}_2\text{CO}_3$ support, which confirmed that Pd nanoparticles had been successfully loaded on $\text{La}_2\text{O}_2\text{CO}_3$ -TNS. HAADF-STEM images and corresponding EDX-elemental mapping images of top-view and side-view of $\text{Pd}/\text{La}_2\text{O}_2\text{CO}_3$ -TNS on edge of carbon lattice were presented in Figure 4e and 4f, respectively. There are three elements in the sample: O (blue), La (orange) and Pd (yellow). Obviously, Pd locates averagely on every surface of $\text{La}_2\text{O}_2\text{CO}_3$ -TNS. Because the top and bottom surface area account for about 70 % of the total area, this $\text{La}_2\text{O}_2\text{CO}_3$ -TNS supported Pd structure is expected to have a large distribution of surface-exposed Pd atoms over top and bottom surface of $\text{La}_2\text{O}_2\text{CO}_3$ -TNS.

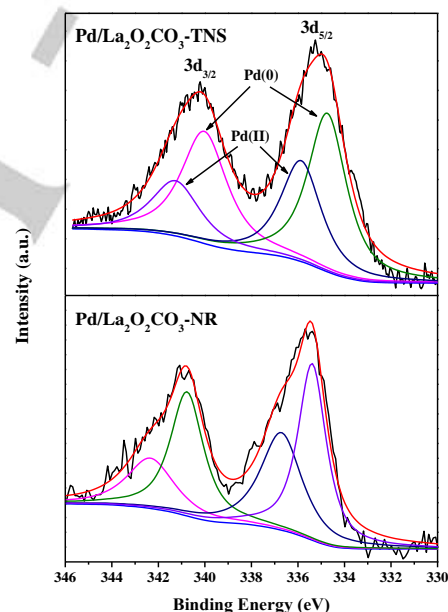


Figure 5. Pd 3d region of XPS spectra of as-prepared $\text{Pd}/\text{La}_2\text{O}_2\text{CO}_3$ -TNS and $\text{Pd}/\text{La}_2\text{O}_2\text{CO}_3$ -NR samples.

Pd 3d region of XPS spectra of as-prepared $\text{Pd}/\text{La}_2\text{O}_2\text{CO}_3$ -TNS and $\text{Pd}/\text{La}_2\text{O}_2\text{CO}_3$ -NR samples was showed in Figure 5, which are deconvoluted into two pairs of doublets. The peaks at 334.8 and 340.1 eV are assigned to the binding energies of Pd(0) $3d_{5/2}$ and $3d_{3/2}$, and these at 335.9 and 341.3 eV are attributed to Pd(II) oxidation state $3d_{5/2}$ and $3d_{3/2}$, respectively, possibly due to the oxidation when exposed to air.^[32] The binding energy of metallic Pd(0) $3d_{5/2}$ of $\text{Pd}/\text{La}_2\text{O}_2\text{CO}_3$ -TNS shifted to lower binding energy by 0.7 eV compared with $\text{Pd}/\text{La}_2\text{O}_2\text{CO}_3$ -NR, indicating weakened 3d electron binding for Pd in the $\text{Pd}/\text{La}_2\text{O}_2\text{CO}_3$ -TNS, which likely results from partial electron transfer from $\text{La}_2\text{O}_2\text{CO}_3$ -TNS to Pd. This electron transfer would increase the electron

density of Pd and enhance the penetration of outer-layer electrons to the inner layer, which changed the binding energies and substantially enhanced the catalytic activity.^[33]

Temperature-programmed desorption of CO₂ (CO₂-TPD) and Temperature-programmed reduction of H₂ (H₂-TPR) profiles of as-prepared Pd/La₂O₂CO₃-TNS and Pd/La₂O₂CO₃-NR catalysts were shown in Figure 6 and Figure 7. Figure 6 showed that two obvious peaks at 110 °C and 280 °C appeared, which were attribute to weak and medium strong basic sites of La₂O₂CO₃, corresponding to surface OH groups and La-O site pairs, respectively.^[34] Compared with Pd/La₂O₂CO₃-NR, as-prepared Pd/La₂O₂CO₃-TNS catalyst exhibited smaller amount of weak and medium-strong basic sites (0.13 mmol g⁻¹). These results suggested that Pd/La₂O₂CO₃-TNS and Pd/La₂O₂CO₃-NR catalysts possessed different surface atomic arrangement. According to previous analysis, due to surface (110) planes exposed mainly, which were made up of O and La atom, Pd/La₂O₂CO₃-NR catalyst showed large amount of weak and medium-strong basic sites (0.21 mmol g⁻¹), which confirmed that oxygen enrichment on surface of Pd/La₂O₂CO₃-TNS catalyst.

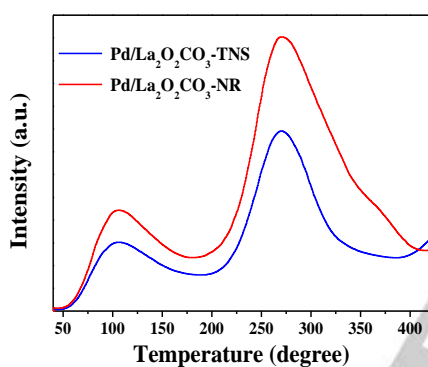


Figure 6. CO₂-TPD profiles of as-prepared Pd/La₂O₂CO₃-TNS and Pd/La₂O₂CO₃-NR catalysts.

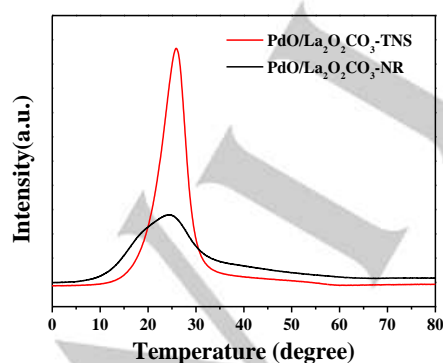


Figure 7. H₂-TPR profiles of as-prepared PdO/La₂O₂CO₃-TNS and PdO/La₂O₂CO₃-NR catalysts.

H₂-TPR was used to investigate the reducibility and nature of noble metal sites of the Pd/La₂O₂CO₃-TNS catalysts, and the H₂-TPR profile was shown in Figure 7. The Pd/La₂O₂CO₃-TNS

catalyst showed two reduction peaks in the temperature region of -10-850 °C. The peaks at high temperature regions can be attributed to the reduction of lattice oxygen of La₂O₂CO₃-TNS support (not shown), whereas the sharp reduction peak below 50 °C could be ascribed to the reduction of PdO_x (to the Pd⁰) and the surface adsorbed oxygen species^[30] and the corresponding H₂ consumption of Pd/La₂O₂CO₃-TNS catalyst was 238 μmol g⁻¹, which was almost two time larger than the theoretical amount for reducing Pd(II) to Pd(0) (96 μmol g⁻¹). The extra H₂ consumption was caused by the oxygen back-spillover from La₂O₂CO₃-TNS to Pd. In addition, the amount of H₂ consumption for this peak for as-prepared Pd/La₂O₂CO₃-NR was 190 μmol g⁻¹, which was lower than Pd/La₂O₂CO₃-TNS, suggesting that a larger amount of high-valence palladium and higher adsorbed oxygen species concentration existed in the Pd/La₂O₂CO₃-TNS sample. The above results demonstrate that the reducibility of the supported Pd-based sample was dependent on the support morphology. Compared to Pd/La₂O₂CO₃-NR catalysts, higher hydrogen consumption might be due to a stronger interaction between a larger amount of coordination-unsaturated surface PdO_x and La₂O₂CO₃-TNS.

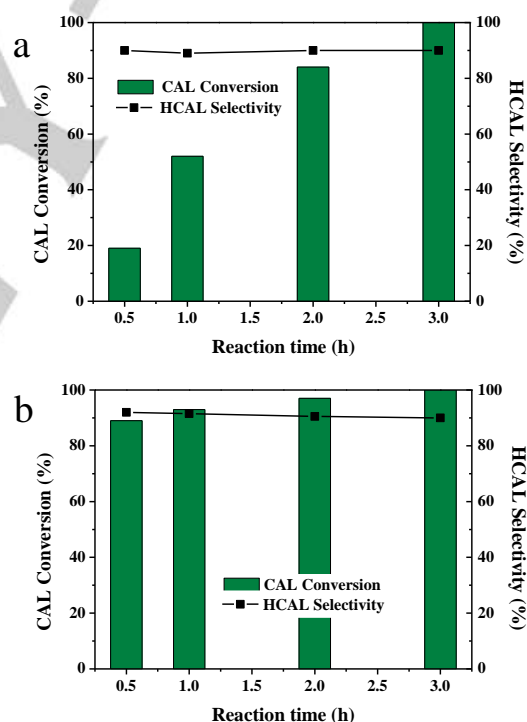


Figure 8. CAL hydrogenation performance over (a) Pd/La₂O₂CO₃-NR and (b) Pd/La₂O₂CO₃-TNS catalysts. Reaction conditions: CAL (1 mL), ethanol (20 mL), catalyst (100 mg), H₂ (1.0 MPa), temperature: 353 K.

The catalytic activity of CAL hydrogenation on the Pd/La₂O₂CO₃-TNS and Pd/La₂O₂CO₃-NR catalysts was evaluated and the reaction time dependence of CAL conversion and HCAL selectivity was shown in Figure 8. Compared with Pd/La₂O₂CO₃-NR catalyst, Pd/La₂O₂CO₃-TNS exhibited significantly excellent catalytic activity on CAL hydrogenation and it accelerates quickly

at 0.5 h, and a complete conversion is achieved at about 1 h. In the current reaction process, high conversion of CAL (90%) and high selectivity of HCAL (92%) were achieved after 0.5 h of reaction time. In addition, we also expressed the activity as turnover frequency (TOF) per mmol surface metal Pd. The Pd/La₂O₂CO₃-TNS catalyst exhibits a TOF = 41238 h⁻¹ in contrast to 1251 h⁻¹ for the Pd/La₂O₂CO₃-NR. This performance results were the one of highest activity for reported heterogeneous hydrogenation catalysts, such as Pd@TNT^[35], Pd-NMC^[36], PdWN/SBA-15^[37] and so on.^[38-43] This result indicated that morphology effect of La₂O₂CO₃ support can modify the reaction rate of CAL hydrogenation.

The catalytic reusability of Pd/La₂O₂CO₃-TNS investigated in a five-run recycling test was shown in Figure 9. No apparent decline of conversion and selectivity happens, reflecting stable activity during the reuse process, which further confirmed that SMSI play important roles in promoting catalytic activity. As shown in Figure 10, Kinetic measurements identified that activation energies of Pd/La₂O₂CO₃-NR was about 100.6 kJ mol⁻¹ whereas Pd/La₂O₂CO₃-TNS was just only 50.9 kJ mol⁻¹. It was observed that morphology-induced SMSI between Pd and La₂O₂CO₃-TNS with the abundant surface oxygen improve reducibility and oxygen mobility and increased the catalytic activity.

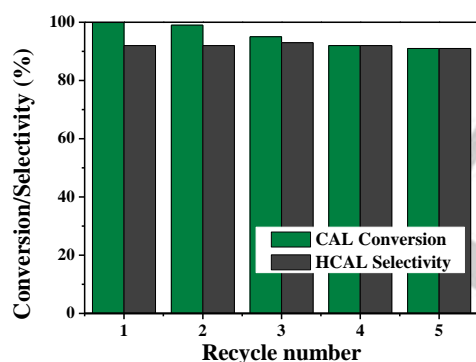


Figure 9. Recycling test of the used Pd/La₂O₂CO₃-TNS catalyst for CAL hydrogenation. Reaction conditions: CAL (1 mL), ethanol (20 mL), catalyst (100 mg), H₂ (1.0 MPa), time: 3 h, temperature: 353 K.

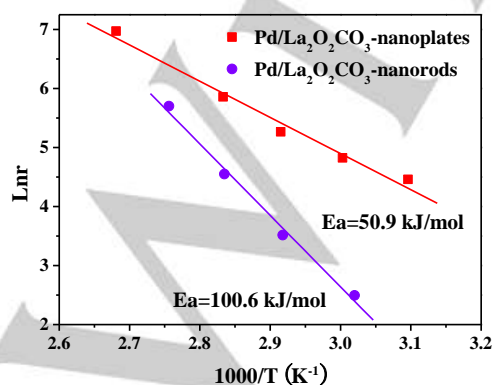


Figure 10. Arrhenius plot of the reaction rate of CAL hydrogenation on the Pd/La₂O₂CO₃-TNS catalyst at 323-373 K.

Conclusion

In summary, we have developed a new triangle-shaped La₂O₂CO₃ nanosheets supported Pd nanoparticles (Pd/La₂O₂CO₃-TNS) catalyst presenting the best catalytic activity with TOF of up to 41238 h⁻¹ than Pd/La₂O₂CO₃-NR catalyst and other previous reported and excellent recycling stability for selective hydrogenation of CAL to HCAL. It was also the first time that triangle-shaped La₂O₂CO₃ was synthesized and used as a support for heterogeneous catalytic reactions. This enhanced activity of Pd/La₂O₂CO₃-TNS resulted from strong metal-support interactions (SMSI). Structure analysis and characterization demonstrated that surface Oxygen-enriched La₂O₂CO₃-TNS supports exposed (001) planes was beneficial to charge transfer between the Pd nanoparticles and triangle-shaped La₂O₂CO₃ nanosheets and increases the electron density of Pd. Moreover, the modulated electron states of the Pd/La₂O₂CO₃-TNS catalysts can enhance the adsorption and activation of hydrogen, leading to the enhanced hydrogenation activity. These discoveries not only open up the development of a new basic oxide supported metal catalyst through morphology-controlled synthesis, but also extend application of the SMSI in basic oxide.

Acknowledgements ((optional))

This work was financially supported by the National Natural Science Foundation of China (No. 21802008, 21503023) and Advanced Catalysis and Green Manufacturing Collaborative Innovation Center, Changzhou University.

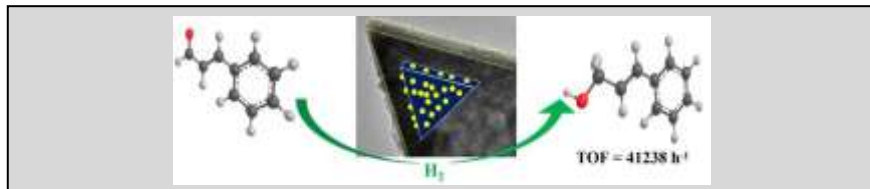
Keywords: Pd/La₂O₂CO₃ • triangular-shaped nanosheets • cinnamaldehyde hydrogenation • Strong metal-supports interaction

- [1] P. Munnik, P. E. de Jongh and K. P. de Jong, *Chem. Rev.* **2015**, *115*, 6687-6781.
- [2] C. Copéret, F. Allouche, K. W. Chan, M. P. Conley, M. F. Delley, A. Fedorov, I. B. Moroz, V. Mougel, M. Pucino, K. Searles, K. Yamamoto and P. A. Zhizhko, *Angew. Chem. Int. Ed.* **2018**, *57*(22), 6398-6440.
- [3] T. Montini, M. Melchionna, M. Monai and P. Fornasier, *Chem. Rev.* **2016**, *116*(10), 5987-6041.
- [4] Z. H. He, Q. L. Qian, J. Ma, Q. L. Meng, H. C. Zhou, J. L. Song, Z. M. Liu and B. X. Han, *Angew. Chem. Int. Ed.* **2016**, *55*(2), 737-741.
- [5] X. Wei, B. Shao, Y. Zhou, Y. Li, C. C. Jin, J. Y. Liu and W. J. Shen, *Angew. Chem. Int. Ed.* **2018**, *57*(35), 11289-11293.
- [6] B. Bai, Q. Qiao, H. Arandiyán, J. H. Li and J. M. Hao, *Environ. Sci. Technol.* **2016**, *50*(5), 2635-2640.
- [7] J. B. Ernst, S. Muratsugu, F. Wang, M. Tada and F. Glorius, *J. Am. Chem. Soc.* **2016**, *138*(34), 10718-10721.

- [8] J. Seth, P. Dubey, V. R. Chaudhari and B. L. V. Prasad, *New J. Chem.* **2018**, *42*(1), 402-410.
- [9] B. Yu, T. Ayvalı, Z. Q. Wang, X. Q. Gong, A. A. Bagabas and S. C. E. Tsang, *Catal. Sci. Technol.* **2019**, *9*, 3435-3444.
- [10] D. M. Marinković, M. V. Stanković, A. V. Veličković, J. M. Avramović, M. R. Miladinović, O. O. Stamenković, V. B. Veljković and D. M. Jovanović, *Renew. Sust. Energ. Rev.* **2016**, *56*, 1387-1408.
- [11] S. Kattel, W. Yu, X. Yang, B. Yan, Y. Huang, W. M. Wan, P. Liu and J. G. Chen, *Angew. Chem. Int. Ed.* **2016**, *55*(28), 7968-7973.
- [12] W. Karim, C. Spreafico, A. Kleibert, J. Gobrecht, J. VandeVondele, Y. Ekinci and J. A. van Bokhoven, *Nature* **2017**, *541*, 68-71.
- [13] S. Oh, Y. K. Kim, C. H. Jung, W. H. Doh and J. Y. Park, *Chem. Commun.* **2018**, *54*, 8174-8177.
- [14] H. F. Yin, C. Wang, H. G. Zhu, S. H. Overbury, S. H. Sun and S. Dai, *Chem. Commun.* **2008**, 4357-4359.
- [15] J. Cho, L. L. Xu, C. Jo and R. Ryoo, *Chem. Commun.* **2017**, *53*, 3810-3813.
- [16] P. Liu, Y. Zhao, R. Qin, S. Mo, G. Chen, L. Gu, D. M. Chevrier, P. Zhang, Q. Guo, D. D. Zang, B. H. Wu, G. Fu and N. F. Zheng, *Science* **2016**, *352*(6287), 797-800.
- [17] S. Zhang, C. R. Chang, Z. Q. Huang, J. Li, Z. Wu, Y. Y. Ma, Z. Y. Zhang, Y. Wang and Y. Q. Qu, *J. Am. Chem. Soc.* **2016**, *138*(8), 2629-2637.
- [18] H. Y. Tan, J. Wang, S. Z. Yu and K. B. Zhou, *Environ. Sci. Technol.* **2015**, *49*, 8675-8682.
- [19] X. Huang, C. Dang, H. Yu, H. Wang and F. Peng, *ACS Catal.* **2015**, *5*(2), 1155-1163.
- [20] J. C. Matsubu, S. Zhang, L. DeRita, N. S. Marinkovic, J. G. Chen, G. W. Graham, X. Q. Pan and P. Christopher, *Nat. Chem.* **2017**, *9*(2), 120-127.
- [21] H. Tang, Y. Su, B. Zhang, A. F. Lee, M. A. Isaacs, K. Wilson, L. Li, Y. G. Ren, J. H. Huang, M. Haruta, B. T. Qiao, X. Liu, C. Z. Jin, D. S. Su, J. H. Wang and T. Zhang, *Sci. Adv.* **2017**, *3*(10), e1700231.
- [22] H. Tang, J. Wei, F. Liu, B. Qiao, X. Pan, L. Li, J. Y. Liu, J. H. Wang and T. Zhang, *J. Am. Chem. Soc.* **2016**, *138*(1), 56-59.
- [23] J. Zhang, H. Wang, L. Wang, S. Ali, C. T. Wang, L. X. Wang, X. J. Meng, B. Li, D. S. Su and F. S. Xiao, *J. Am. Chem. Soc.* **2019**, *141*(7), 2975-2983.
- [24] Y. Guo, S. Mei, K. Yuan, D. J. Wang, H. C. Liu, C. H. Yan and Y. W. Zhang, *ACS Catal.* **2018**, *8*(7), 6203-6215.
- [25] A. L. Chen, X. Yu, Y. Zhou, S. Miao, Y. Li, S. Kuld, J. Sehested, J. Y. Liu, T. Aoki, S. Hong, M. F. Camellone, S. Fabris, J. Ning, C. C. Jin, C. W. Yang, A. Nefedov, C. Wöll, Y. M. Wang and W. J. Shen, *Nat. Catal.* **2019**, *2*, 334-341.
- [26] W. T. Figueiredo, G. B. Della Mea, M. Segala, D. L. Baptista, C. Escudero, V. Pérez-Dieste and F. Bernardi, *ACS Appl. Nano Mater.* **2019**, *2*(4), 2559-2573.
- [27] R. Xu, X. Wang, D. Wang, K. Zhou and Y. D. Li, *J. Catal.* **2006**, *237*(2), 426-430.
- [28] E. W. Zhao, H. Zheng, K. Ludden, Y. Xin, H. E. Hagelin-Weaver, C. R. Bowers, *ACS Catal.*, **2016**, *6*(2), 974-978.
- [29] F. Wang, R. J. Shi, Z. Q. Liu, P. J. Shang, X. Y. Pang, S. Shen, Z. C. Feng, C. Li and W. J. Shen, *ACS Catal.* **2013**, *3*(5), 890-894.
- [30] K. Murata, Y. Mahara, J. Ohyama, Y. Yamamoto, S. Arai and A. Satsuma, *Angew. Chem. Int. Ed.* **2017**, *56*(50), 15993-15997.
- [31] F. Wang, Z. N. Zhang, X. J. Wei, Q. H. Fang and X. M. Jiang, *Appl. Catal. A* **2017**, *543*, 196-200.
- [32] Y. Y. Zeng, B. W. Wang, Y. Li, X. L. Yan, L. G. Chen and Y. Wang, *Ind. Eng. Chem. Res.* **2020**, *59*(4), 1436-1445.
- [33] N. Ullah, M. Imran, K. Liang, C. Z. Yuan, A. Zeb, N. Jiang, U. Y. Qazi, S. Sahar and A. W. Xu, *Nanoscale* **2017**, *9*, 13800-13807.
- [34] F. Wang, N. Ta, Y. Li, W. J. Shen, *Chin. J. Catal.* **2014**, *35*, 437-443.
- [35] X. Yang, L. Wu, L. Ma, X. Li, T. Wang, S. Liao, *Catal. Commun.* **2015**, *59*, 184-188.
- [36] A. S. Nagpure, L. Gurralla, P. Gogoi, S. V. Chilukuri, *RSC Adv.* **2016**, *6*, 44333-44340.
- [37] D. Wang, Y. Zhu, C. Tian, L. Wang, W. Zhou, Y. L. Dong, H. J. Yan, H. G. Fu, *ChemCatChem* **2016**, *8*, 1718-1726.
- [38] M. J. Martínez - Ortiz, M. A. de la Rosa-Guzmán, J. R. Vargas-García, J. L. Flores-Moreno, N. Castillo, A. Guzmán-Vargas, S. Morandi, R. M. Pérez-Gutiérrez, *Can. J. Chem. Eng.* **2018**, *96*, 297-306.
- [39] W. Lin, H. Cheng, L. He, Y. Yu, F. Zhao, *J. Catal.* **2013**, *303*, 110-116.
- [40] X. J. Ni, B. S. Zhang, C. Li, M. Pang, D. S. Su, C. T. Williams, C. H. Liang, *Catal. Commun.* **2012**, *24*, 65-69.
- [41] X. Chen, M. Li, J. C. Guan, X. K. Wang, C. T. Williams, C. H. Liang, *Ind. Eng. Chem. Res.* **2012**, *51*, 3604-3611.
- [42] C. Antonetti, L. Toniolo, G. Cavinato, C. Forte, C. Ghignoli, R. Ishak, F. Cavani, A. M. R. Galletti, *Appl. Catal. A* **2015**, *496*, 40-50.
- [43] H. Gu, X. Xu, A. Chen, P. Ao, X. Yan, *Catal. Commun.* **2013**, *41*, 65-69.

Entry for the Table of Contents

Insert graphic for Table of Contents here. ((Please ensure your graphic is in **one** of following formats))



A triangular-shaped $\text{La}_2\text{O}_2\text{CO}_3$ nanosheets exposed the predominant (001) planes supported Pd catalyst ($\text{Pd}/\text{La}_2\text{O}_2\text{CO}_3\text{-TNS}$) was successfully prepared, which exhibited highly active and recycling ability for hydrogenation of cinnamaldehyde with TOF of up to 41238 h^{-1} . Existence of morphology-induced strong metal and basic support interaction state in $\text{Pd}/\text{La}_2\text{O}_2\text{CO}_3\text{-TNS}$ significantly enhances reaction activity.